

Fault-tolerant Control of a Wind Turbine with a Squirrel-cage Induction Generator and Rotor Bar Defects

DOI 10.7305/automatika.54-3.189
UDK 681.532.5.09:621.313.33(621.224)
IFAC 2.1.4; 5.5.4

Original scientific paper

Wind turbines are usually installed on remote locations and in order to increase their economic competence malfunctions should be reduced and prevented. Faults of wind turbine generator electromechanical parts are common and very expensive. This paper proposes a fault-tolerant control strategy for variable-speed variable-pitch wind turbines in case of identified and characterised squirrel-cage generator rotor bar defect. An upgrade of the torque control loop with flux-angle-based torque modulation is proposed. In order to avoid or to postpone generator cage defects, usage of pitch controller in the low wind speed region is introduced. Presented fault-tolerant control strategy is developed taking into account its modular implementation and installation in available control systems of existing wind turbines to extend their life cycle and energy production. Practical implementation aspects such as estimation of variables used in control and estimate errors are considered and respected in operation, as well as fault-induced asymmetries. Simulation results for the case of a megawatt class wind turbine and the identified rotor bar fault are presented.

Key words: Wind turbine control, Torque control, Generator fault-tolerant control, Nonlinear estimation, Asymmetric field-oriented control

Upravljanje vjetroagregatom otporno na oštećenja kaveza asinkronog generatora. Vjetroagregati se obično postavljaju na udaljene, nepristupačne lokacije te je potrebno spriječiti nastanak kvarova da bi se povećala njihova ekonomska konkurentnost. Kvarovi elektromehaničkih dijelova generatora vjetroagregata česti su i vrlo skupi. U ovom radu predstavljen je koncept upravljanja vjetroagregatima s promjenjivom brzinom vrtnje i zakretom lopatica za slučaj identificiranog i okarakteriziranog oštećenja kaveza asinkronog generatora. Predložena je nadogradnja na postojeći algoritam upravljanja momentom zasnovana na njegovoj modulaciji s obzirom na položaj magnetskog toka generatora. Da bi se izbjeglo ili usporilo širenje napuknuća kaveza generatora, predložena je primjena regulacijskog kruga za zakret lopatica i u režimu rada vjetroagregata ispod nazivne brzine vrtnje. Predstavljena strategija upravljanja razvijena je uvažavajući mogućnost modularnog nadovezivanja na postojeće metode upravljanja već postavljenih vjetroagregata s ciljem produženja njihova životnog vijeka i povećanja proizvodnje energije. Razmatrani su i uvaženi aspekti vezani uz praktičnu izvedbu, kao što je estimacija varijabli korištenih u upravljačkom algoritmu i pripadajuće pogreške estimata, kao i nesimetrije uzrokovane nastankom kvara. U radu su dani simulacijski rezultati za slučaj vjetroagregata iz megawatne klase s dijagnosticiranim napuknućem kaveza rotora.

Ključne riječi: upravljanje vjetroagregatom, upravljanje momentom, upravljanje otporno na kvarove generatora, nelinearna estimacija, vektorsko upravljanje nesimetričnog stroja

1 INTRODUCTION

Aspiration for finding adequate substitute for conventional fossil fuel power systems has a great impact on today political and economic trends and guidelines. Combining different branches of science and engineering, wind energy is one of the fastest-growing renewable energy sources with an average growth rate of 26% in last 5 years [1]. It is green, inexhaustible, everywhere available but unreliable with poor power quality and as a result – expensive.

The challenge is to make wind turbine control system capable of maximising the energy production and the produced energy quality while minimising costs of installation and maintenance.

Wind turbines are usually installed at low-turbulent-wind remote locations and it is important to avoid very costly unscheduled repairs. In order to improve reliability of wind turbines, different fault-tolerant control (FTC) algorithms have been introduced [2], focused mainly on sen-

sor, inverter and actuator faults. Focus here is on generator electromechanical faults, which are besides gearbox and power converters faults the most common in wind turbine systems [3]. Many installed wind turbines have squirrel-cage induction generator (SCIG) and about 20% to 30% of machine faults are caused by defects in rotor cage [4].

Rotor bar defect is caused by thermal fatigue due to cyclic thermal stress on the endring-bar connection which occurs because of different thermal coefficients of bars and lamination steel. As presented in [5, 6], a monitoring system that is able to detect a developing bar defect is designed based on current signature analysis and offers the possibility to switch from preventive to predictive maintenance and thus to significantly reduce costs.

Focus of this paper is to research and develop a fault-tolerant extension of the wind turbine control system that prevents the identified rotor bar defect from spreading. We introduce a fast control loop for flux-angle-based modulation of the generator torque, and a slow control loop that ensures the generator placement at a point that enables the fast loop to perform correctly and keeps the electrical energy production optimal under emergency circumstances.

The basic concept of the generator FTC is proposed in [7]. Here we further improve the idea and develop the algorithm by considering practical implementation aspects such as how state estimation techniques are combined with the derived FTC strategy. State estimation error is anticipated in the FTC in order to guarantee safe operation in its presence. Unscented Kalman filter approach is chosen for estimation of variables that are needed in wind turbine generator torque control because of its proficient ability to cope with hard nonlinearities. A paper that concerns with influence of parameter variation on machine control and their estimation is presented in [8].

Occurred rotor bar fault introduces changes in classical mathematical model of the induction machine. A method for modeling changes in machine leakage inductance is proposed and the fault influence is respected in the control. The method presents an upgrade of conventional fundamental-wave approach in machine modeling and control. A similar work related with asymmetries caused by a stator inter-turn fault can be found in [9].

This paper is organized as follows. The basic control strategy for a variable-speed variable-pitch wind turbine is presented in Section 2 along with normal wind turbine operating maps. In Section 3 a mathematical model of an SCIG is given explaining the theoretical basis used to form a control system extension. Estimation of machine variables used for torque control is described in Section 4. A fault-tolerant approach and control algorithm are proposed and presented in Section 5. They enable wind turbine operation in emergency state with estimation error

taken into account. Section 6 concerns with changes of the SCIG model due to occurred fault. Section 7 provides MATLAB/Simulink simulation results obtained with the proposed fault-tolerant control strategy.

2 WIND TURBINE CONTROL SYSTEM

Variable-speed variable-pitch wind turbine operating area is parted into two regions (see Fig. 1): low-wind-speed region (region I), where all the available wind power is fully captured and high-wind-speed region (region II) where the power output is maintained constant while reducing the aerodynamic torque and keeping generator speed at the rated value.

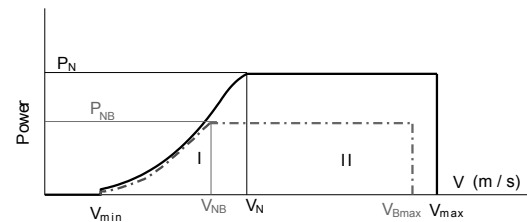


Fig. 1. Ideal power curve with maximum P_N and power curve due to developed fault with maximum P_{NB}

The ability of a wind turbine to capture wind energy is expressed through a power coefficient C_P , which is defined as the ratio of extracted power P_t to wind power P_V :

$$C_P = \frac{P_t}{P_V}. \quad (1)$$

The maximum value of C_P , known as Betz limit, is $C_{Pmax} = 0.593$. It defines the maximum theoretical capability of wind power capture. The real power coefficient of modern commercial wind turbines reaches values of about 0.48 [10]. Power coefficient data is usually given as a function of the tip-speed-ratio λ and pitch angle β (Fig. 2). Turbine power and torque are given by [11]:

$$P_t = C_P(\lambda, \beta) P_V = \frac{1}{2} \rho_{air} R^2 \pi C_P(\lambda, \beta) V^3, \quad (2)$$

$$T_t = \frac{P_t}{\omega} = \frac{1}{2} \rho_{air} R^3 \pi C_Q(\lambda, \beta) V^2, \quad (3)$$

where $C_Q = C_P/\lambda$, ρ_{air} , R , V and ω are torque coefficient, air density, radius of the aerodynamic disk of a wind turbine, wind speed and the angular speed of blades, respectively, and $\lambda = \frac{\omega R}{V}$.

Since the goal is to maximise the output power in low-wind-speed region, wind turbine must operate such that the power coefficient C_P is at its maximum value (or near it). This is achieved by maintaining λ and β on values that ensure $C_P = C_{Pmax}$ [10–12], see Fig. 2. Therefore the

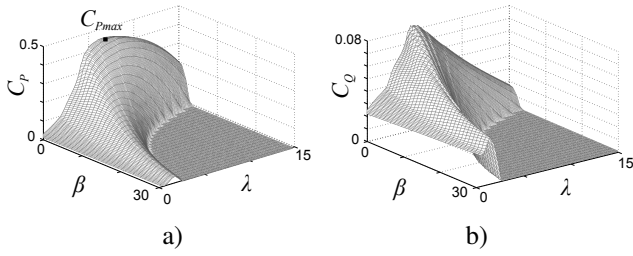


Fig. 2. Power a) and torque b) coefficients for an exemplary 700 kW variable-speed variable-pitch wind turbine

generator torque and consequently the aerodynamic torque is determined by:

$$T_{gref} = \frac{1}{2\lambda_{opt}^3 n_s^3} \rho_{air} \pi R^5 C_{Pmax} \omega_g^2 = K_\lambda \omega_g^2, \quad (4)$$

where n_s is the gearbox ratio. This way the wind turbine operating points in low wind speed region are located at the maximum output power curve, called C_{Pmax} locus. This $T_{gref} = K_\lambda \omega_g^2$ torque controller (Fig. 3) can be easily realized using a simple look-up table.

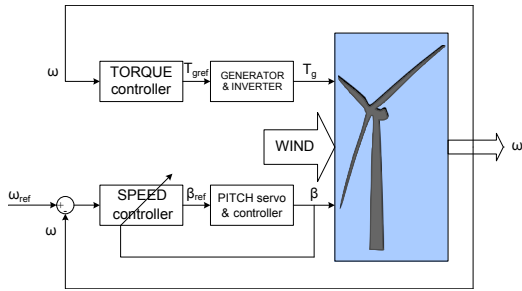


Fig. 3. Control system of a variable-speed variable-pitch wind turbine

Above the designated rated wind speed, task of the control system is to maintain the output power of the wind turbine constant. This can be done by reducing the aerodynamic torque and angular speed of blades by rotating them along their longitudinal axis (pitching). Consequently, the wind turbine power coefficient is reduced. A proportional-integral (PI) or proportional-integral-derivative (PID) controller with gain-scheduling technique is often satisfactory for pitch control (Fig. 3).

3 MATHEMATICAL MODEL OF AN INDUCTION MACHINE

There are several approaches in modelling an induction machine [13]. One of the most common is the representation of machine stator and rotor phases in the two-phase common rotating (d, q) coordinate system, which is suitable

for field-oriented control application. A rotor-based field-oriented control (RFOC) implies that the common rotating (d, q) frame is aligned with rotor flux linkage:

$$\bar{\psi}_r = \psi_{rd} + j0, \quad (5)$$

and the complex value of $\bar{\psi}_r$ becomes a scalar ψ_{rd} .

Mathematical model of a squirrel-cage induction machine used for RFOC can be represented with the following equations [13]:

$$u_{sd} = k_s i_{sd} + L_l \frac{di_{sd}}{dt} + \left(\frac{L_l}{T_r} - \frac{L_s}{T_r} \right) i_{mr} - \omega_e L_l i_{sq}, \quad (6)$$

$$u_{sq} = R_s i_{sq} + L_l \frac{di_{sq}}{dt} - \omega_e (L_l - L_s) i_{mr} + \omega_e L_l i_{sd}, \quad (7)$$

where $u_{sd,q}$ are stator voltages in d and q axes, $i_{sd,q}$ are stator currents, i_{mr} is the rotor magnetizing current. Parameter $T_r = \frac{L_r}{R_r}$ is the rotor time constant, parameters L_r , L_s and L_m are rotor, stator and mutual inductance, respectively, R_r and R_s are rotor and stator resistances, $L_l = (L_s - \frac{L_m^2}{L_r})$, $k_s = (R_s - \frac{L_l}{T_r} + \frac{L_s}{T_r})$. Variable $\omega_e = 2\pi f$ denotes the speed of machine magnetizing flux rotation with respect to the stator, where f is the frequency of voltage supplied by the inverter. Terms with ω_e in (6) and (7) represent the machine back-electromotive force (EMF).

RFOC equations are given by:

$$i_{mr} = \frac{\psi_{rd}}{L_m}, \quad (8)$$

$$i_{sd} = i_{mr} + T_r \frac{di_{mr}}{dt}, \quad (9)$$

$$\omega_{sl} = \omega_e - p\omega_g, \quad (10)$$

$$T_g = \frac{3}{2} p \frac{L_m^2}{L_r} i_{mr} i_{sq} = k_m i_{mr} i_{sq}, \quad (11)$$

where $\omega_{sl} = \frac{i_{sq}}{T_r i_{mr}}$ is the slip speed calculated as a difference between the magnetic flux rotation speed ω_e and real rotor mechanical speed ω_g multiplied by the number of stator pole pairs p . The variable ω_{sl} with its sign dictates whether the asynchronous machine is in the motor or in the generator operating regime.

Relation (11) is the key equation for RFOC of an induction machine. Following from (9), the magnetizing current vector i_{mr} is not suitable for fast control action influencing torque because of the time lag T_r . Therefore it is kept constant in the sub-nominal speed operating region and $i_{mr} \triangleq i_{sd} \triangleq i_{sdn}$ is implied, where i_{sdn} is the rated value of d -current corresponding to the rated flux value. Torque is controlled only by q stator current component (i_{sq}).

Relations (6) and (7) show that d and q coordinates are not fully decoupled for the case of voltage-controlled machine (Fig. 4) and changing the voltage value in one axis

affects also the other axis. Since it would be very complicated to control these coupled voltages, a decoupling method is applied (see [13]). By introducing correction voltages Δu_{sd} and Δu_{sq} :

$$\Delta u_{sd} = - \left(\frac{L_l}{T_r} - \frac{L_s}{T_r} \right) i_{mr} + \omega_e L_l i_{sq}, \quad (12)$$

$$\Delta u_{sq} = \omega_e (L_l - L_s) i_{mr} - \omega_e L_l i_{sd}, \quad (13)$$

fully decoupled relations are derived:

$$u_{sd} + \Delta u_{sd} = k_s i_{sd} + L_l \frac{di_{sd}}{dt}, \quad (14)$$

$$u_{sq} + \Delta u_{sq} = R_s i_{sq} + L_l \frac{di_{sq}}{dt}. \quad (15)$$

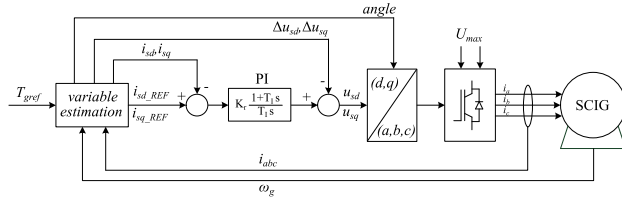


Fig. 4. Field-oriented control loop

These equations are now suitable for further design of the control loop and PI controllers are chosen with integral time constants $T_{Id} = L_l/k_s$ for d -current, $T_{Iq} = L_l/R_s$ for q -current and gain K_r . Finally, closed loop dynamics can now be represented as first-order lag system with transfer function:

$$\frac{T_g(s)}{T_{gref}(s)} = \frac{i_{sq}(s)}{i_{sq_REF}(s)} = \frac{1}{1 + \tau s}, \quad (16)$$

where τ is a time constant defined with $\tau = \frac{\sigma L_s}{K_r}$. The slip speed is proportional to the torque (or i_{sq} current):

$$\omega_{sl} = \frac{i_{sq}}{T_r i_{mr}} = \frac{1}{T_r k_m i_{mr}^2} T_g = k T_g. \quad (17)$$

Fastest achievable transient of currents is determined with inverter limitation. Considering the worst case scenario, the highest output of q -current PI controller is attained at the beginning of the transient with value of $u_{sq} + \Delta u_{sq} = K_r (i_{sq_REF} - i_{sq})$. Respecting the maximum available voltage supplied to one phase $U_{max} \approx U_{sq_max}$, the minimum and maximum reference values of q -current and therefore torque can be roughly calculated, respectively as:

$$T_1 = \frac{1}{K_r k_g} (-U_{max} - k_e \omega_e) - T_0, \quad (18)$$

$$T_2 = \frac{1}{K_r k_g} (U_{max} - k_e \omega_e) + T_0, \quad (19)$$

where $k_g = k_m i_{sdn}$, $k_e = L_s i_{sdn}$ and T_0 is the torque starting point for the transient. Notice that back EMF supports torque reduction and aggravates torque restoration. Fast transients with T_1 and T_2 are needed for achieving the maximum possible power production with proposed fault-tolerant control. However, in digital control implementation torque in the next discretization step must not exceed desired reference value. Therefore the value of T_1 (absolute value of which is by far greater than one of T_2) is limited with:

$$T_1 = T_0 - (T_0 - T_d) \frac{\tau}{T_s}, \quad (20)$$

where T_d is the desired torque value and T_s is the sample time.

4 ESTIMATION OF FIELD-ORIENTED CONTROL VARIABLES

Field-oriented control and its derivatives require precise machine magnetizing flux position and it is impossible to measure it in asynchronous machines. If the flux position used in calculations deviates from the real flux position, (d, q) coordinate system becomes unaligned and relation (8) is no longer valid, which introduces error and mathematical model discrepancy. In the sequel we propose an estimation method for obtaining FOC variables based on the unscented Kalman filter (UKF) algorithm.

4.1 Stochastic machine model

For the implementation of estimation algorithm, a stochastic nonlinear mathematical model is required. Therefore, the model from Section 3 is augmented to include process and measurement noise v and n , respectively:

$$\frac{di_{sd}}{dt} = \frac{1}{L_l} u_{sd} + \frac{1}{L_l} \Delta u_{sd} - \frac{k_s}{L_l} i_{sd} + v_1, \quad (21)$$

$$\frac{di_{sq}}{dt} = \frac{1}{L_l} u_{sq} + \frac{1}{L_l} \Delta u_{sq} - \frac{R_s}{L_l} i_{sq} + v_2, \quad (22)$$

$$\frac{di_{mr}}{dt} = \frac{1}{T_r} (i_{sd} - i_{mr}) + v_3, \quad (23)$$

$$\frac{d\rho}{dt} = p\omega_g + \frac{1}{T_r} \frac{i_{sq}}{i_{mr}} + v_4, \quad (24)$$

where ρ is the flux angle. Described model can be generally represented as:

$$\dot{x} = F_c(x, u, v), \quad (25)$$

where $x = [i_{sd} \ i_{sq} \ i_{mr} \ \rho]^T$ is the state vector, $u = [u_{sd} \ u_{sq} \ \omega_g]^T$ is the input vector and $F_c(\cdot)$ is a vector function. Stator currents are usually measured in electric machines and measurement vector is therefore chosen as $y = [i_a \ i_b]^T$ (the sum $i_a + i_b + i_c = 0$ holds), generally represented as:

$$y = H(x, n). \quad (26)$$

The measurement vector is related with d, q coordinate system through inverse Clark's and Park's transforms [13]:

$$i_a = i_{sd} \cos \rho - i_{sq} \sin \rho + n_1, \quad (27)$$

$$i_b = i_{sd} \left(-\frac{1}{2} \cos \rho + \frac{\sqrt{3}}{2} \sin \rho \right) + i_{sq} \left(\frac{1}{2} \sin \rho + \frac{\sqrt{3}}{2} \cos \rho \right) + n_2. \quad (28)$$

Control scheme for FOC with UKF and corresponding input and measurement vectors is presented in Fig. 5.

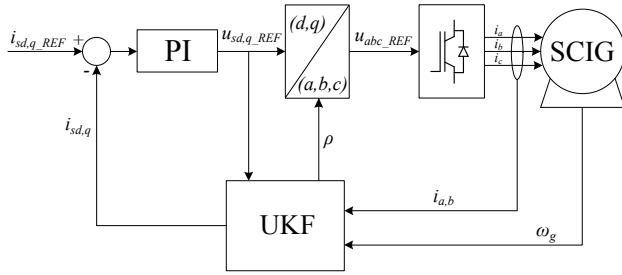


Fig. 5. Field-oriented control loop with unscented Kalman filter (UKF)

4.2 Unscented Kalman filter algorithm

The UKF represents a novel approach for estimations in nonlinear systems and provides better results than extended Kalman filter (EKF) in terms of mean estimate and estimate covariance [14]. The core idea of UKF lies in unscented transformation, the way of propagating Gaussian random variables (GRV) through a nonlinear mapping. The unscented transformation is performed using so-called sigma points, a minimal set of carefully chosen sample points that enables better capturing of mean and covariance of GRVs than simple point-linearization of the mapping: posterior mean and covariance are accurate to the second order of the Taylor series expansion for any non-linearity as proven in [15].

An attractive feature of UKF is that partial derivatives and Jacobian matrix (like in EKF) are not needed and continuous-time nonlinear dynamics equations are directly used in the filter, without discretization or linearization. Computational effort of UKF with carefully implemented algorithm can be similar to that of the EKF. More information can be found in [14] and [15] while different applications of UKF are presented in [16, 17]. The UKF algorithm is given in the sequel.

4.2.1 Initialization and time update

In order to choose a proper set of sigma points, the estimated state vector \hat{x}_k in a discrete time-instant k is

augmented to include means of process and measurement noise \bar{v} and \bar{n} , forming the vector \hat{x}_k^a :

$$\hat{x}_k^a = \mathbb{E}(x_k^a) = [\hat{x}_k^T \bar{v} \bar{n}]^T, \quad (29)$$

where $\mathbb{E}(\cdot)$ denotes the expectance. Covariance matrix \mathbf{P}_k is also augmented accordingly and \mathbf{P}_k^a is formed:

$$\mathbf{P}_k^a = \mathbb{E}((x_k^a - \hat{x}_k^a)^T (x_k^a - \hat{x}_k^a)) = \begin{bmatrix} \mathbf{P}_k & \mathbf{0} & \mathbf{0} \\ \mathbf{0} & \mathbf{R}^v & \mathbf{0} \\ \mathbf{0} & \mathbf{0} & \mathbf{R}^n \end{bmatrix}, \quad (30)$$

where \mathbf{R}^v and \mathbf{R}^n are process and measurement noise covariance matrices, respectively. Time update algorithm starts with the unscented transformation and by forming the sigma points matrix \mathcal{X}_k^a :

$$\mathcal{X}_k^a = \begin{bmatrix} \hat{x}_k^a & \hat{x}_k^a + \gamma \sqrt{\mathbf{P}_k^a} & \hat{x}_k^a - \gamma \sqrt{\mathbf{P}_k^a} \end{bmatrix}. \quad (31)$$

Variable $\sqrt{\mathbf{P}_k^a}$ is the lower-triangular Cholesky factorization of matrix \mathbf{P}_k^a and $\gamma = \sqrt{L + \lambda}$ is a scaling factor. Parameter L is the dimension of augmented state x_k^a and parameter λ determines the spread of sigma points around the current estimate, calculated as:

$$\lambda = \alpha^2 (L + \kappa) - L. \quad (32)$$

Parameter α is usually set to a small positive value e.g. $10^{-4} \leq \alpha \leq 1$ and κ is usually set to 1. There are $2L + 1$ sigma points used for transformation, which correspond to dimension of vector $\mathcal{X}_k^a = [(\mathcal{X}_k^x)^T (\mathcal{X}_k^v)^T (\mathcal{X}_k^n)^T]^T$.

Time-update equations used to calculate prediction of states \hat{x}_{k+1}^- and state covariance \mathbf{P}_{k+1}^- as well as prediction of outputs \hat{y}_{k+1}^- are:

$$\mathcal{X}_{i,k+1|k}^x = F_d(\mathcal{X}_{i,k}^x, u_k, \mathcal{X}_{i,k}^v), \quad i = 0, \dots, 2L, \quad (33)$$

$$\hat{x}_{k+1}^- = \sum_{i=0}^{2L} W_i^{(m)} \mathcal{X}_{i,k+1|k}^x, \quad (34)$$

$$\mathbf{P}_{k+1}^- = \sum_{i=0}^{2L} W_i^{(c)} \left(\mathcal{X}_{i,k+1|k}^x - \hat{x}_{k+1}^- \right) \times \left(\mathcal{X}_{i,k+1|k}^x - \hat{x}_{k+1}^- \right)^T, \quad (35)$$

$$\mathcal{Y}_{i,k+1|k} = H \left(\mathcal{X}_{i,k+1|k}^x, \mathcal{X}_{i,k}^n \right), \quad i = 0, \dots, 2L, \quad (36)$$

$$\hat{y}_{k+1}^- = \sum_{i=0}^{2L} W_i^{(m)} \mathcal{Y}_{i,k+1|k}, \quad (37)$$

where i is an index of columns in vector \mathcal{X}_k^a (and $\mathcal{X}_k^x, \mathcal{X}_k^v, \mathcal{X}_k^n$) starting from zero value. Weights for mean and covariance calculations are given by:

$$\begin{aligned} W_0^{(m)} &= \frac{\lambda}{(L + \lambda)}, \\ W_0^{(c)} &= \frac{\lambda}{(L + \lambda)} + (1 - \alpha^2 + \beta), \\ W_i^{(m)} &= W_i^{(c)} = \frac{\lambda}{2(L + \lambda)}, \quad i = 1, \dots, 2L. \end{aligned} \quad (38)$$

For Gaussian distributions, $\beta = 2$ is optimal.

4.2.2 Measurement update

Once required covariance and cross-covariance matrices are computed by employing unscented transformation, the measurement update algorithm is performed in the same way as in classical EKF:

$$\mathbf{P}_{\tilde{y}_{k+1}\tilde{y}_{k+1}} = \sum_{i=0}^{2L} W_i^{(c)} (\mathcal{Y}_{i,k+1|k} - \hat{y}_{k+1}^-) \times (\mathcal{Y}_{i,k+1|k} - \hat{y}_{k+1}^-)^T, \quad (39)$$

$$\mathbf{P}_{\tilde{x}_{k+1}\tilde{y}_{k+1}} = \sum_{i=0}^{2L} W_i^{(c)} (\mathcal{X}_{i,k+1|k}^x - \hat{x}_{k+1}^-) \times (\mathcal{Y}_{i,k+1|k} - \hat{y}_{k+1}^-)^T, \quad (40)$$

$$\mathbf{K}_{k+1} = \mathbf{P}_{\tilde{x}_{k+1}\tilde{y}_{k+1}} \mathbf{P}_{\tilde{y}_{k+1}\tilde{y}_{k+1}}^{-1}, \quad (41)$$

$$\hat{x}_{k+1} = \hat{x}_{k+1}^- + \mathbf{K}_{k+1} (y_{k+1} - \hat{y}_{k+1}^-), \quad (42)$$

$$\mathbf{P}_{k+1} = \mathbf{P}_{k+1}^- - \mathbf{K}_{k+1} \mathbf{P}_{\tilde{y}_{k+1}\tilde{y}_{k+1}} \mathbf{K}_{k+1}^T, \quad (43)$$

where $\mathbf{P}_{\tilde{y}_{k+1}\tilde{y}_{k+1}}$ is output covariance matrix, $\mathbf{P}_{\tilde{x}_{k+1}\tilde{y}_{k+1}}$ is cross-covariance matrix, \mathbf{K}_{k+1} is Kalman gain matrix, \hat{x}_{k+1} are posterior states and \mathbf{P}_{k+1} is posterior covariance.

5 FAULT-TOLERANT CONTROL

Previous sections have described most widely adopted wind turbine control strategies, as well as mathematical model of the generator. This section is dedicated for further improvement of control strategies in order to disable or to postpone generator fault development and to achieve maximum energy production under emergency conditions at the same time. For now, detected generator fault triggers a turbine safety device and leads to a system shut-down. Whole unscheduled repair process requires significant amounts of money and the situation is even worse for off-shore wind turbines, not to mention opportunity costs of turned-off wind turbine.

To avoid thermal stress of the defected rotor bar, currents flowing through it should be less than currents flowing through the healthy ones. The magnitude of currents in rotor bar is sinusoidal and it is determined by the machine magnetic flux. Speed at which the flux rotates along the rotor circumference is the generator slip speed defined with (10). Flux position with respect to the rotor is denoted with θ . The flux affects the damaged rotor bar only on a small part of its path as it moves along the circumference, whereas this path part is denoted with $\Delta\theta = \theta_2 - \theta_1$, see Fig. 6. Our primary goal is to reduce the electrical and thermal stress reflected through currents and corresponding generator torque in that angle span to the maximum

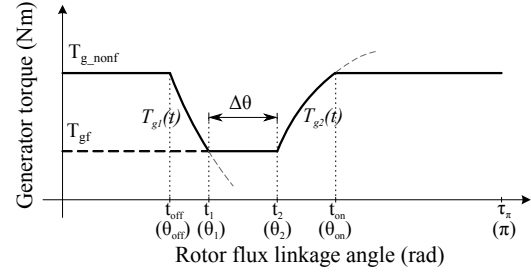


Fig. 6. Torque modulation due to a fault condition. In brackets are angles attained at denoted time instant.

allowed safety value T_{gf} . The value T_{gf} is determined based on fault identification through machine fault monitoring and characterisation techniques, together with flux angles θ_1 and θ_2 [5]. Related topic, focused on stator winding inter-turn short circuit faults and periodically modulated stator flux is proposed in [18] and [19].

Torque is therefore modulated based on the machine flux angular position with respect to the damaged part as shown in Fig. 6. When the flux in angle θ approaches the angle span $\Delta\theta$, the torque is reduced to the maximum allowed value T_{gf} defined with a fault condition. After the flux passes it, the torque is restored to the right selected value T_{g_nonf} . The value T_{g_nonf} is determined such that the average machine torque is maintained on the optimum level, taking into account the machine constraints. Procedure is then periodically executed, with period equal π (or τ_π in time domain), since the flux influences the faulty part with its north and south pole in each turn.

Using the described FOC algorithm with decoupling procedure the generator is modelled as first-order lag system, as mentioned in Section 3. Torque transients from Fig. 6 are therefore defined as exponential functions, decrease and increase respectively:

$$T_{g1}(t) = e^{-\frac{t}{\tau}} (T_{g_nonf} - T_1) + T_1, \quad (44)$$

$$T_{g2}(t) = T_2 - e^{-\frac{t}{\tau}} (T_2 - T_{gf}). \quad (45)$$

Slip speed of the generator is defined as

$$\omega_{sl}(T_g(t)) = \frac{d\theta}{dt}, \quad (46)$$

from which the angle is obtained:

$$\theta(t) - \theta(0) = \int_0^t \omega_{sl}(T_g(t)) dt = \int_0^t k T_g(t) dt. \quad (47)$$

Desired T_{gf} is reached with transient (44) at certain time t_1 and desired T_{g_nonf} is reached with transient (45)

at certain time t_{on} :

$$T_{gf} = e^{-\frac{t_1 - t_{off}}{\tau}} (T_{g_nonf} - T_1) + T_1, \quad (48)$$

$$T_{g_nonf} = T_2 - e^{-\frac{t_{on} - t_2}{\tau}} (T_2 - T_{gf}). \quad (49)$$

The angle span which has passed during the torque reduction determines the angle θ_{off} at which the transition has to start in order to reach the torque T_{gf} at angle θ_1 due to the finite bandwidth of the torque control loop. In the same way torque restoration transient determines the angle θ_{on} at which the torque T_{g_nonf} is fully restored. Finally, θ_{off} is derived from (18), (47) and (48):

$$\theta_{off} = \theta_1 - k\tau (T_{g_nonf} - T_{gf} - T_1 \ln a), \quad (50)$$

where $\ln a = \ln \frac{T_{gf} - T_1}{T_{g_nonf} - T_1}$. In the same way, θ_{on} is obtained as:

$$\theta_{on} = \theta_2 + k\tau (T_{gf} - T_{g_nonf} - T_2 \ln b), \quad (51)$$

where $\ln b = \ln \frac{T_2 - T_{g_nonf}}{T_2 - T_{gf}}$.

If the torque value T_{g_nonf} can be restored at some angle then the following relation holds:

$$\theta_{on} - \theta_{off} \leq \pi. \quad (52)$$

Putting (50) and (51) into (52), the following is obtained for condition (52):

$$-k\tau (T_1 \ln a + T_2 \ln b) \leq \pi - \Delta\theta. \quad (53)$$

Because of large inertia of the whole drivetrain, generator and blade system, described torque oscillations (reduction and restoration) are barely noticeable on the speed transient, such that the wind turbine shaft perceives the mean torque value:

$$T_{av} = \frac{1}{\tau_\pi} \int_0^{\tau_\pi} T_g dt. \quad (54)$$

Mean value of the generator torque from Fig. 6 is then given by:

$$T_{av} = \frac{\pi - 2k\tau (T_1 \ln a + T_2 \ln b)}{k\tau_\pi}, \quad (55)$$

with

$$\tau_\pi = \frac{\pi - \Delta\theta + k\tau (T_1 \ln a + T_2 \ln b)}{kT_{g_nonf}} - \tau (\ln a + \ln b) + \frac{\Delta\theta}{kT_{gf}}. \quad (56)$$

By applying torque (and corresponding q -current) references T_1 and T_2 from (18), (19), it is ensured that the generator spends the least possible time in reduced torque area.

Equation (52) (or (53)) is not satisfied if the speed ω_g is large enough (or if there is a large rotor path under fault influence). In that case the torque modulation is given with Fig. 7 and peak torque T_g^* is attained at angle θ^* :

$$\begin{aligned} \theta_2 - \pi + k\tau (T_{gf} - T_g^* - T_2 \ln b^*) &= \\ &= \theta_1 - k\tau (T_g^* - T_{gf} - T_1 \ln a^*), \end{aligned} \quad (57)$$

where $\ln a^* = \ln \frac{T_{gf} - T_1}{T_g^* - T_1}$ and $\ln b^* = \ln \frac{T_2 - T_g^*}{T_2 - T_{gf}}$. Values T_g^* and θ^* can be obtained from:

$$k\tau (T_1 \ln a^* + T_2 \ln b^*) = \Delta\theta - \pi, \quad (58)$$

$$\theta^* = \theta_1 - k\tau (T_g^* - T_{gf} - T_1 \ln a^*). \quad (59)$$

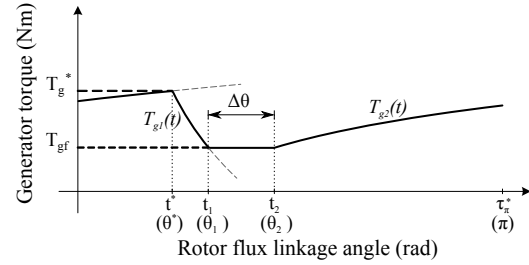


Fig. 7. Torque modulation due to a fault condition when T_{g_nonf} cannot be restored

Mean value of the generator torque from Fig. 7 (i.e. in case when (52) is not satisfied) is now given by

$$T_{av} = \frac{\pi - k\tau (T_1 \ln a^* + T_2 \ln b^*)}{k\tau_\pi^*}, \quad (60)$$

with

$$\tau_\pi^* = -\tau (\ln a^* + \ln b^*) + \frac{\Delta\theta}{kT_{gf}}. \quad (61)$$

Concludingly, if (53) is fulfilled, the resulting average torque is given with (55); if not, then the resulting average torque is given with (60). On the boundary, i.e. for equality in (52) or (53), both (55) and (60) give the same torque T_{av} , such that $T_{av}(\omega_g)$ is continuous. The maximum available torque T_{g_nonf} is the nominal generator torque T_{gn} . Replacing T_{g_nonf} in (55) with the nominal generator torque T_{gn} gives the maximum available average torque under fault characterised with $\Delta\theta$ and T_{gf} . Fig. 8 shows an exemplary graph of available speed-torque points under machine fault, where the upper limit is based on relations (53), (55) and (60) with $T_{g_nonf} = T_{gn}$. Dashed area denotes all available average generator torque values that can be achieved for certain generator speed.

From Fig. 8 it follows that up to the speed ω_{g1} it is possible to control the wind turbine in the faulty case without

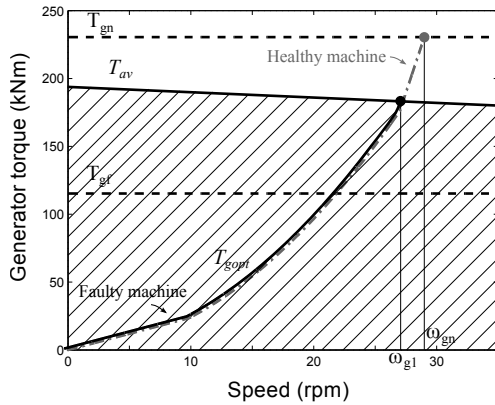


Fig. 8. Available torque-speed generator operating points under fault condition (shaded area). Full line is the achievable part of the wind turbine torque-speed curve under faulty condition. Dash-dot line is the healthy machine curve.

sacrificing power production. However, from that speed onwards it is necessary to use blades pitching in order to limit the aerodynamic torque and to keep the power production below optimal such that fault spreading is suppressed. The speed control loop is modified such that instead of reference ω_n the reference ω_1 (in case of gearbox, $\omega_1 = \omega_{g1}/n_s$) is selected. This activates pitch control once the right edge of the feasible-under-fault optimal torque characteristics is reached. The interventions in classical wind turbine control that ensure fault-tolerant control are given in Fig. 9. Algorithms of the slow and the fast fault-tolerant control loop are given in the sequel. The fast loop is executed at each discrete time step, while the slow loop is performed once after every torque modulation period τ_π .

Algorithm 1 Fault-tolerant control algorithm, slow loop

- I. If $T'_{gref} \leq T_{gf}$, disable the fast loop and pass T'_{gref} to the torque controller;
- II. Compute T_{g_nonf} from (18), (19), (55) and (56) such that $T_{av}(\omega_g) = T'_{gref}$; if $T_{g_nonf} > T_{gn}$, set $T_{g_nonf} = T_{gn}$;
- III. If (53) is fulfilled set $\theta_{start} = \theta_{off} \bmod \pi$ and $\theta_{end} = \theta_{on}$ else compute θ^* from (59) and set $\theta_{start} = \theta^* \bmod \pi$, $\theta_{end} = \theta_2$ and $T_{g_nonf} = T_2$;
- IV. Compute ω_{g1} as a speed coordinate of the intersection point of $T_{av}(\omega_g)$ and of the normal wind turbine torque controller characteristics, compute $\omega_1 = \omega_{g1}/n_s$ and set $\omega_{ref} = \omega_1$.

Algorithm 2 Fault-tolerant control algorithm, fast loop

I. On the positive edge of logical conditions:

- $\theta > \theta_{start}$ set $T_{gref} = T_1$,
- $\theta > \theta_1$ set $T_{gref} = T_{gf}$,
- $\theta > \theta_2$ set $T_{gref} = T_2$,
- $\theta > \theta_{end}$ set $T_{gref} = T_{g_nonf}$.

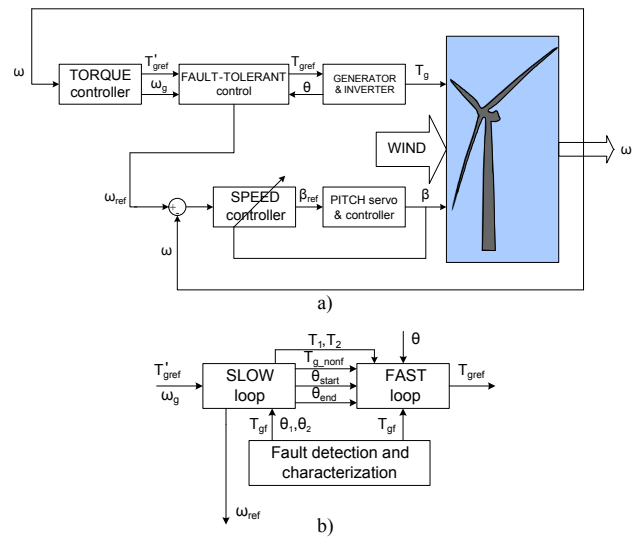


Fig. 9. a) Control system of wind turbine with fault-tolerant control strategy. b) Enlarged fault-tolerant control block.

5.1 Uncertainties

Considering practical aspects of the algorithm implementation, a look-up table with T_{g_nonf} values can be used. Exponential torque transients can be approximated with straight lines for lower computational efforts as in [7]. The real generator stator current measurements used for UKF correction procedure are noisy and the model used for estimation may deviate from the real generator system. Proposed fault-tolerant control algorithm is based on the accurate information about machine magnetizing flux position θ . Therefore, if θ is not correct, the torque is not reduced appropriately on the faulty part $\Delta\theta$ and rotor-bar defect tends to spread further on.

To overcome the problem, faulty part $\Delta\theta$ can be redundantly extended to ensure the proper torque reduction in the faulty machine section, making the FTC algorithm robust on the error of flux position estimate. For that purpose we propose to include the flux position uncertainty obtained from the estimation algorithm and state covariance matrix in θ_{off} and θ_{on} calculations procedure. Faulty part $\Delta\theta$ is extended by $\pm 3\sigma_\theta$, where σ_θ is a square root of

the variance of machine flux position estimate $\hat{\theta}$ extracted from the covariance matrix in (43). Probability that the true flux position is within the presumed interval is:

$$p\left(\theta \in \left[\hat{\theta} - 3\sigma_\theta\right], \theta \in \left[\hat{\theta} + 3\sigma_\theta\right]\right) = 99.73\%. \quad (62)$$

Another feature of the presented FTC algorithm is that torque reduction at point θ_{off} always starts at fixed time step dictated by the sample time T_s . Therefore, it may miss the intended angle of θ_{off} and begin at some point $\theta_{off} + \Delta\theta_{T_s}$. Depending on the sample time value this feature can have a noticeable effect as well. Following from (46), $\Delta\theta_{T_s}$ is calculated as:

$$\Delta\theta_{T_s} = \omega_{sl}T_s = kT_{g_nonf}T_s. \quad (63)$$

In the same manner, uncertainty of the fault detection algorithm can also be taken into consideration, formed as a variance σ_{θ_1} . All of described uncertainties are included in θ_{off}^c and θ_{on} calculations with corrected values of θ_1^c and θ_2^c :

$$\theta_1^c = \theta_1 - 3\sigma_\theta - \Delta\theta_{T_s} - 3\sigma_{\theta_1}, \quad (64)$$

$$\theta_2^c = \theta_2 + 3\sigma_\theta + \Delta\theta_{T_s} + 3\sigma_{\theta_2}. \quad (65)$$

That way, equations (50) and (51) with θ_1^c and θ_2^c remain unchanged.

6 CONTROL OF AN INDUCTION MACHINE WITH ROTOR ASYMMETRIES

In Section 3 a widely-adopted and well-tested RFOC algorithm is described. It is based on so-called fundamental wave machine model approach, which assumes ideal and sinusoidal distribution of magnetizing flux in the machine air-gap. It provides very good results and satisfying performance of the machine but neglects inherent asymmetries due to machine physics and geometry.

Because of occurred rotor bar defect, newly formed asymmetries are introduced inside machine rotor phases. They are reflected on the system performance in terms of vibrations, as well as current and torque oscillations. The diagnostics method for locating and characterisation of the rotor bar defect proposed in [5, 6] is based on observation of this newly arisen system performance.

This section is dedicated for further improvement of system performance and smooth operation of the slightly asymmetric generator. Rotor bar defect causes very small change in resistance R_r and inductance L_r of the whole rotor cage, but has a noticeable impact on the leakage inductance L_l . In order to respect asymmetries in machine control we propose an extension of the previously described RFOC algorithm based on the variable leakage inductance observation.

For symmetric machine the leakage inductance is the same for all phases and so far the L_l was implied to be a constant parameter. Due to occurred asymmetry in the machine, the leakage inductance is no longer the same for all phases and can be represented with a complex value denoted with $\bar{L}_{l,t}$. It is composed of a scalar offset value L_{offset} and a complex value \bar{L}_{mod} . The offset value represents the symmetric part while complex value includes induced asymmetry with its magnitude and spatial direction. More about this approach can be found in [5, 6]. In common (d, q) reference frame leakage inductance $L_{l,t}$ is represented as:

$$\bar{L}_{l,t} = L_{offset} + \bar{L}_{mod}, \quad \bar{L}_{mod} = L_{mod} \cdot e^{j2\gamma}. \quad (66)$$

The angle $\gamma = \omega_{sl}t + \varphi$ corresponds to the current location of the rotor bar defect with respect to the magnetizing flux. The frequency is doubled due to effects of both north and south magnetic field poles per single flux revolution period. Both L_{mod} and γ are provided from the fault monitoring and characterisation technique.

The leakage inductance can be represented with:

$$\bar{L}_{l,t} = L_{ld} + j \cdot L_{lq}, \quad (67)$$

where $L_{ld} = L_{offset} + L_{mod} \cos(2\gamma)$, and $L_{lq} = L_{mod} \sin(2\gamma)$.

By putting it into stator and rotor voltage equations (6) and (7) and by performing linear transformations of equalities, the following relations are obtained:

$$\begin{aligned} u_{sd} &= k_a i_{sd} + L_a \frac{di_{sd}}{dt} + \frac{L_{lq}}{L_{ld}} R_s i_{sq} - \frac{L_{lq}}{L_{ld}} u_{sq} - \\ &\quad - \omega_e L_a i_{sq} + \left(\frac{L_a}{T_r} - \frac{L_s}{T_r}\right) i_{mr} + \omega_e \frac{L_{lq}}{L_{ld}} L_s i_{mr}, \end{aligned} \quad (68)$$

$$\begin{aligned} u_{sq} &= R_s i_{sq} + L_a \frac{di_{sq}}{dt} - \left(\frac{L_{lq}}{L_{ld}} R_s + \frac{L_{lq}}{L_{ld}} \frac{L_s}{T_r}\right) i_{sd} + \\ &\quad + \frac{L_{lq}}{L_{ld}} u_{sd} + \omega_e L_a i_{sd} + \frac{L_{lq}}{L_{ld}} \frac{L_s}{T_r} i_{mr} - \\ &\quad - \omega_e (L_a - L_s) i_{mr}, \end{aligned} \quad (69)$$

where $k_a = (R_s - \frac{L_a}{T_r} + \frac{L_s}{T_r})$ and $L_a = (L_{ld} + \frac{L_{lq}^2}{L_{ld}})$. In the same way as in symmetric FOC, the decoupling method is applied. By introducing correction voltages Δu_{sd} and Δu_{sq} , fully decoupled relations are derived:

$$u_{sd} + \Delta u_{sd} = k_a i_{sd} + L_a \frac{di_{sd}}{dt}, \quad (70)$$

$$u_{sq} + \Delta u_{sq} = R_s i_{sq} + L_a \frac{di_{sq}}{dt}, \quad (71)$$

where

$$\Delta u_{sd} = \frac{L_{lq}}{L_{ld}} u_{sq} - \frac{L_{lq}}{L_{ld}} R_s i_{sq} + \omega_e L_a i_{sq} - \left(\frac{L_a}{T_r} - \frac{L_s}{T_r} \right) i_{mr} - \omega_e \frac{L_{lq}}{L_{ld}} L_s i_{mr}, \quad (72)$$

$$\Delta u_{sq} = -\frac{L_{lq}}{L_{ld}} u_{sd} + \left(\frac{L_{lq}}{L_{ld}} R_s + \frac{L_{lq}}{L_{ld}} \frac{L_s}{T_r} \right) i_{sd} - \omega_e L_a i_{sd} - \frac{L_{lq}}{L_{ld}} \frac{L_s}{T_r} i_{mr} + \omega_e (L_a - L_s) i_{mr}. \quad (73)$$

Equations (68)-(73) represent the mathematical model of an asymmetric induction machine. With complex leakage inductance from (66) and (67), influence of the rotor bar defect is respected in the machine control. With $L_{ld} = L_{offset} = L_l$ and $L_{lq} = 0$ above relations are valid for symmetric machine and obtain the same form as in (6)-(15).

In the same manner, PI controller parameters are chosen with integral time constants $T_{Ida} = L_a/k_a$ for d -current, $T_{Iqa} = L_a/R_s$ for q -current. With index 'a' controller parameters in case of detected asymmetry are denoted. PI controller gain K_{ra} is selected with respect to desired transient velocity and inverter constraints. Control system block scheme remains the same as in Fig. 4. The way of detecting the true value of transient leakage inductance $\bar{L}_{l,t}$ under asymmetric machine conditions determines how much is the system performance improved with the new FOC algorithm.

7 SIMULATION RESULTS

This section provides simulation results for a 700 kW MATLAB/Simulink variable-speed variable-pitch wind turbine model with a two-pole 5.5 kW SCIG scaled to match the torque of 700 kW machine. Generator parameters are: $L_s = L_r = 0.112$ H, $L_m = 0.11$ H, $R_s = 0.3304$ Ω , $R_r = 0.2334$ Ω and PI controller gain is $K_r = 1$. Turbine parameters are: $C_{Pmax} = 0.4745$, $R = 25$ m, $\lambda_{opt} = 7.4$, $\omega_n = 29$ rpm, $T_{tn} = 230.5$ kNm with gearbox ratio $n_s = 105.77$. Maximum voltage supplied to one phase is $U_{max} = \frac{2}{3} U_{dc} = 467$ V. Fault is simulated between flux angles $\theta_1 = \frac{\pi}{2}$ and $\theta_2 = \frac{\pi}{2} + \frac{\pi}{5}$, with $T_{gf} = 0.5 T_{gn}$ and presented fault-tolerant control algorithm is applied. Larger sample time is generally more suitable for Kalman filter but here is chosen to fulfil requirements of FOC and fast FTC loop as $T_s = 400$ μ s. Results in Fig. 10 show how the wind turbine behaves in healthy and faulty condition for a linear change of wind speed through the entire wind turbine operating area. As a result of FTC, new nominal operating point is $(\omega_{g1}, T_{av}(\omega_{g1}))$ (Fig. 8) and pitch control is activated sooner than in healthy machine conditions.

Fig. 11 shows the fault-tolerant control system reaction to the fault that is identified at $t = 50$ s for the case when the average generator torque under fault $T_{av}(\omega_g)$ can be equal to the required torque T'_{gref} for the incurred speed ω_g , i.e. the optimum speed-torque point is for the occurred fault in the dashed area of Fig. 8, above the line $T_g = T_{gf}$. A turbulent wind flow based on the Kaimal model is used in the simulations. Fig. 11 also shows that proposed FTC strategy introduces additional wind turbine speed oscillations that influence the whole wind turbine system. A conventional method for avoiding wind turbine resonant frequencies [10–12] can be applied in this case as well. In particular, the torque modulation occurs with frequency of about 2 Hz for rated slip value and contributes to material fatigue. Therefore, the proposed FTC algorithm is to be preferably used only as an emergency reaction until next scheduled overhaul. However, in presented simulations we used a rather serious fault case with T_{gf} being half of rated torque value. In practice, the fault development can be characterised at early stage and T_{gf} is expected to be much closer to T_{gn} and oscillations would be less pronounced.

Fig. 12 shows the fault-tolerant control system reaction to the fault identified at $t = 50$ s for the case when the incurred healthy machine speed-torque operating point falls out of the dashed area of Fig. 8. In this case blade pitching is used in the faulty condition to bring the speed-torque operating point into $(\omega_{g1}, T_{av}(\omega_{g1}))$. Simulations are also performed on a wind turbine with detailed struc-

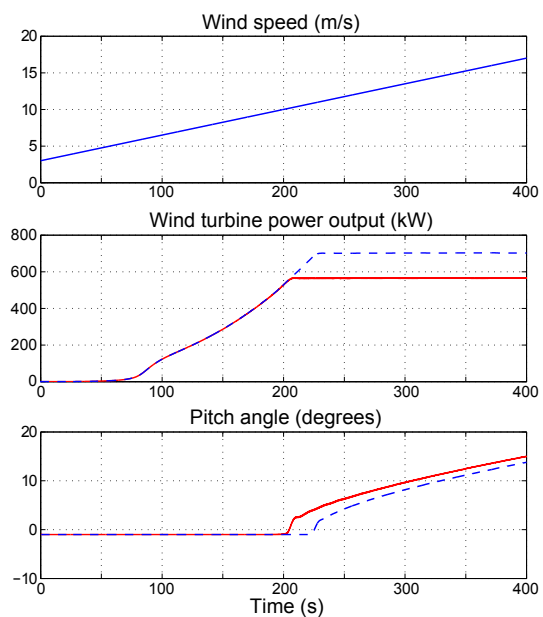


Fig. 10. Wind turbine power production and pitch angle for healthy (dashed line) and faulty conditions

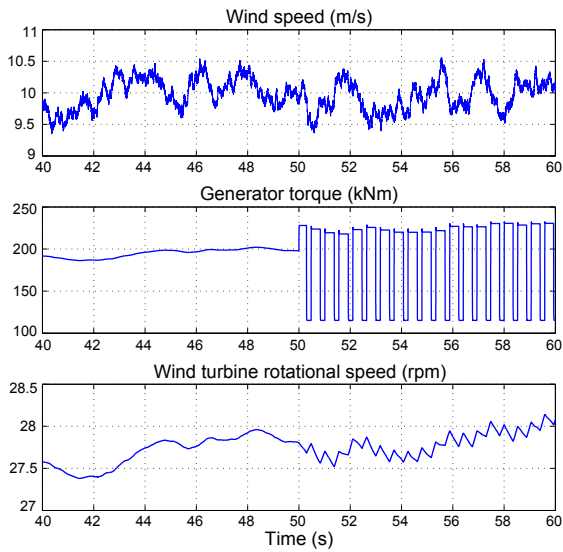


Fig. 11. Generator torque modulation and wind turbine speed when $T_{g_nonf} < T_{gn}$. Fault occurs at 50 s.

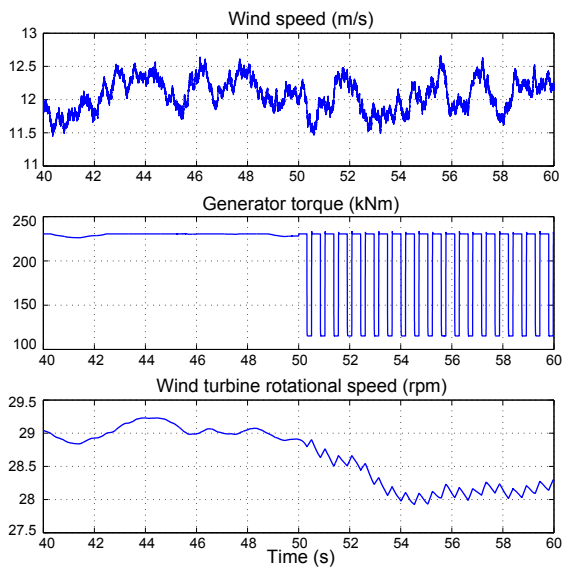


Fig. 12. Generator torque modulation and wind turbine speed when $T_{g_nonf} = T_{gn}$. Fault occurs at 50 s.

tural loads model included. Comparison of a healthy and a faulty (with applied FTC) wind turbine for the same conditions is presented in Fig. 13. Results show that mostly influenced structural points are the top of the wind turbine tower and corresponding bending torque in the x -axis as well as nacelle and blade deflections in the y axis. Coordinate systems are observed according to [20].

Uncertainty of the flux angle estimate is also used in the control procedure. Estimate error ($\hat{\theta} - \theta$) and corresponding variance σ_{θ}^2 are shown in Fig. 14. Measurement noise of

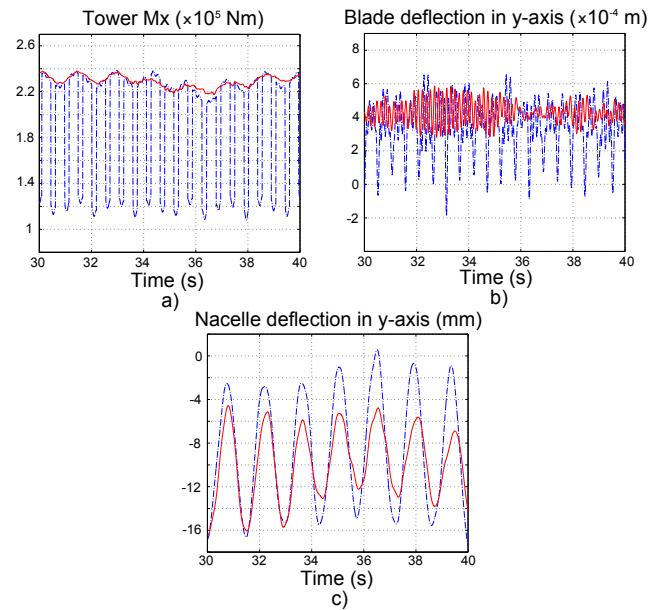


Fig. 13. Wind turbine structural loads for the case of normal operation and applied FTC (dash-dot line). a) presents the bending torque at tower top, b) is y -axis deflection of a blade, with 1 m distance from the blade root, c) is the nacelle deflection in y -axis.

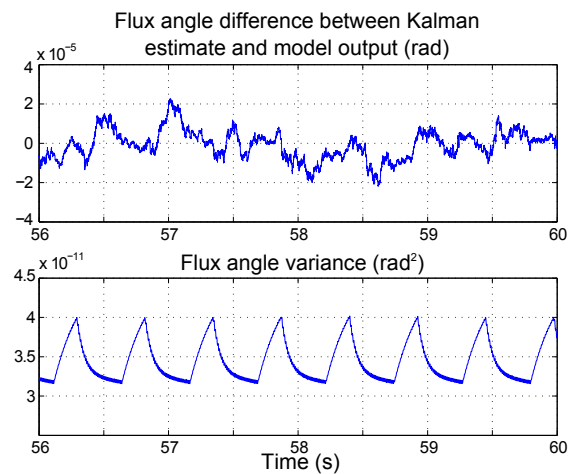


Fig. 14. Flux angle estimation error and variance σ_{θ}^2

± 20 mA has been included in the model. Influence of both flux angle estimate variance and sample time on θ_1 and θ_2 is less than 1% for the case of ideal machine model.

Fig. 15 shows the influence of fast loop reference switching on generator torque. This way the time needed for torque transients is reduced to minimum possible value, which keeps wind turbine in low-energy production operation as little as possible under emergency circumstances.

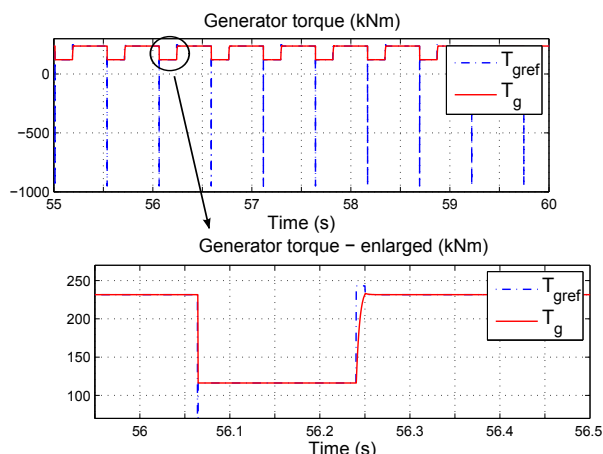


Fig. 15. Generator torque transients

8 CONCLUSION

This paper introduces a fault-tolerant control scheme for variable-speed variable-pitch wind turbines with a squirrel-cage induction generator. We focus on generator rotor bar defect that can be characterised at early stage of development. Presented method is used as an autonomous control reaction to diagnosed fault in order to avoid wind turbine shut-down. Results show that simple extension of the conventional wind turbine control structure prevents the fault propagation while power delivery under fault is deteriorated as less as possible compared to healthy machine conditions. State estimation errors and fault-introduced asymmetries are respected in operation as well.

ACKNOWLEDGEMENT

The research leading to these results has received funding from the European Community's Seventh Framework Programme under grant agreement no 285939 (ACROSS) and from the European Commission and the Republic of Croatia under grant FP7-SEE-ERA.net PLUS ERA 80/01, project MONGS - Monitoring of Wind Turbine Generator Systems.

REFERENCES

- [1] Renewable Energy Policy Network for the 21st Century (REN21), "Renewables 2012," Global status report, 2012.
- [2] S. Pourmohammad, A. Fekih, "Fault-tolerant Control of Wind Turbine Systems - A Review," *Proc. of the 2011. IEEE Green Technologies Conference (IEEE-Green)*, April 2011.
- [3] Z. Daneshi-Far, G. A. Capolino, H. Henao, "Review of Failures and Condition Monitoring in Wind Turbine Generators," *XIX International Conference on Electrical Machines - ICEM 2010*, Sept. 2010.
- [4] A. H. Bonnet and C. Yung, "Increased Efficiency Versus Increased Reliability," *IEEE Industry Applications Magazine*, vol.14, no.1, pp. 29-36, 2008.
- [5] G. Stojičić, P. Nussbaumer, G. Joksimović, M. Vašak, N. Perić and T. M. Wolbank, "Precise Separation of Inherent Induction Machine Asymmetries from Rotor Bar Fault Indicator," *8th IEEE International Symposium on Diagnostics for Electrical Machines, Power Electronics & Drives, SDEMPED*, pp. 9-15, Sept. 2011.
- [6] G. Stojičić, M. Samonig, P. Nussbaumer, G. Joksimović, M. Vašak, N. Perić and T. M. Wolbank, "Monitoring of Rotor Bar Faults in Induction Generators with Full-size Inverter," *Proceedings of the 14th European Conference on Power Electronics and Applications, EPE*, pp. 1-8, Aug.-Sept. 2011.
- [7] V. Lešić, M. Vašak, N. Perić, T. M. Wolbank and G. Joksimović, "Fault-Tolerant Control of a Blade-pitch Wind Turbine With Inverter-fed Generator," *20th IEEE International Symposium on Industrial Electronics, ISIE*, pp. 2097-2102, June 2011.
- [8] V. Lešić, M. Vašak, G. Stojičić, N. Perić, G. Joksimović and T. M. Wolbank, "State and Parameter Estimation for Field-oriented Control of Induction Machine Based on Unscented Kalman Filter," *International Symposium on Power Electronics, Electrical Drives, Automation and Motion, SPEEDAM*, June 2012.
- [9] V. Lešić, M. Vašak, M. Gulin, N. Perić, G. Joksimović and T. M. Wolbank, "Field-oriented Control of an Induction Machine with Winding Asymmetries," *15th International Power Electronics and Motion Control Conference, EPE-PEMC 2012 ECCE Europe*, pp. LS7b-1.2-1-7, Sept. 2012.
- [10] M. Jelavić, "Wind Turbine Control for Structural Dynamic Loads Reduction (in Croatian)," PhD Thesis, Faculty of Electrical Engineering and Computing, University of Zagreb, 2009.
- [11] F. D. Bianchi, H. De Battista and R. J. Mantz, *Wind Turbine Control Systems - Principles, Modelling and Gain Scheduling Design*, London: Springer, ISBN 1-84628-492-9, 2007.
- [12] T. Burton, D. Sharpe, N. Jenkins and E. Bossanyi, *Wind Energy Handbook*, London: John Wiley & Sons, ISBN 0-471-48997-2, 2001.
- [13] M. P. Kazmierkowski, F. Blaabjerg and R. Krishnan, *Control in Power Electronics - Selected Problems*, San Diego, California: Academic Press, An imprint of Elsevier Science, ISBN 0-12-402772-5, 2002.
- [14] S. J. Julier and J. K. Uhlmann, *A General Method for Approximating Nonlinear Transformations of Probability Distributions*, Technical report, Dept. of Engineering Science, University of Oxford, Nov. 1996.
- [15] E. A. Wan and R. van der Merwe, "The Unscented Kalman Filter" in *Kalman Filtering and Neural Networks*. S. Haykin, Ed. New York: John Wiley & Sons, ISBN 0-471-36998-5, 2001.

- [16] M. Vašak, M. Baotić, I. Petrović and N. Perić, "Electronic Throttle State Estimation and Hybrid Theory Based Optimal Control", *Proceedings of the IEEE International Symposium on Industrial Electronics ISIE 2004*, pp. 323-328, May 2004.
- [17] M. Doumiati, A. Victorino, A. Charara and D. Lechner, "Onboard Real-Time Estimation of Vehicle Lateral Tire-Road Forces and Sideslip Angle", *IEEE/ASME Transactions on Mechatronics*, vol. 16, no. 4, pp. 601-614, 2010.
- [18] V. Lešić, M. Vašak, N. Perić, G. Joksimović and T. M. Wolbank, "Fault-tolerant Control of a Wind Turbine with a Squirrel-cage Induction Generator and Stator Inter-turn Faults", *The 12th International Workshop on Advanced Motion Control, AMC*, 6 pages, March 2012.



Vinko Lešić received his master degree in electrical engineering and information technology from University of Zagreb Faculty of Electrical Engineering and Computing (UNIZG-FER) in 2010. Currently, he is with the Department of Control and Computer Engineering at UNIZG-FER where he is pursuing his PhD degree. His research interests are in the area of control theory with application to advanced control of electrical drives and wind turbine generators.



Mario Vašak is an Assistant Professor at the Department of Control and Computer Engineering of University of Zagreb Faculty of Electrical Engineering and Computing (UNIZG-FER). He received his PhD degree in Electrical Engineering from UNIZG-FER in 2007. He works in the areas of predictive/robust/fault-tolerant control and computational geometry applied to them, in the following application domains: renewable energy systems, water management systems, energy-efficient buildings, energy-efficient railway transportation and automotive systems. On behalf of UNIZG-FER he led an FP7-SEE-ERA.net PLUS research project MONGS on generator-fault-tolerant control in wind turbines, and currently he is UNIZG-FER leader of the FP7-STREP UrbanWater that deals with fresh water supply system management in urban environments. He published over 50 papers in journals and conference proceedings.



Nedjeljko Perić received the B.Sc., M.Sc. and Ph.D. degrees in Electrical Engineering from the University of Zagreb Faculty of Electrical Engineering and Computing (UNIZG-FER) in 1973, 1980, and 1989, respectively. From 1973 to 1993 he worked at the Institute of Electrical Engineering of the Končar Corporation, Croatia, as an R&D engineer, Head of the Positioning Systems Department, and Manager of the Automation Section. In 1993 he joined the Department of Control and Computer Engineering at UNIZG-FER as an associate professor. He was appointed as a full professor in 1997 and since 2010 he serves as UNIZG-FER dean. His current research interests are in the fields of process identification and advanced control techniques. In periods 1992-1998 and 2000-2011 he served as the Chairman of KoREMA, the Croatian Society for Communications, Computing, Electronics, Measurements and Control. He is also a member of several international professional associations. Professor Perić is a Fellow of Croatian Academy of Engineering.

- [19] V. Lešić, M. Vašak, N. Perić, G. Joksimović and T. M. Wolbank, "Fault-tolerant Control of a Wind Turbine with Generator Stator Inter-turn Faults", *Automatika*, vol. 54, no. 1, pp. 89-102, 2013.
- [20] Germanischer Lloyd Industrial Services GmbH, "Guideline for the Certification of Wind Turbines", 2010.



Thomas M. Wolbank received the doctoral degree and the Habilitation from Vienna University of Technology, Vienna, Austria, in 1996 and 2004, respectively. Currently, he is with the Department of Energy Systems and Electrical Drives, Vienna University of Technology, Vienna, Austria. He has co-authored some 100 papers in refereed journals and international conferences. His research interests include saliency-based sensorless control of AC drives, dynamic properties and condition monitoring of inverter-fed machines, transient electrical behavior of AC machines, motor drives and their components as well as controlling them by the use of intelligent control algorithms.



Gojko M. Joksimović received PhD degree and the Full Professor degree from University of Montenegro, Montenegro, in 2000 and 2011, respectively. His main research areas include analysis of electrical machines, condition monitoring of electrical machines, and power electronics and control. He is the author of a few books and more than 50 papers published in leading international scientific journals and international conferences.

AUTHORS' ADDRESSES

Vinko Lešić, M.Sc.

Asst. Prof. Mario Vašak, Ph.D.

Prof. Nedjeljko Perić, Ph.D.

**Department of Control and Computer Engineering,
Faculty of Electrical Engineering and Computing,
University of Zagreb,
Unska 3, HR-10000, Zagreb, Croatia**

email: {vinko.lesic,mario.vasak,nedjeljko.peric}@fer.hr

Prof. Thomas M. Wolbank, Ph.D.

**Institute of Energy Systems and Electrical Drives,
Faculty of Electrical Engineering and Information
Technology,**

**Vienna University of Technology,
Gusshausstrasse 25/370-2, AT-1040, Vienna, Austria**
email: thomas.wolbank@tuwien.ac.at

Prof. Gojko M. Joksimović, Ph.D.

**Faculty of Electrical Engineering,
University of Montenegro,
Džordža Vašingtona bb, ME-81000, Podgorica, Montenegro**
email: joxo@ac.me

Received: 2012-01-31

Accepted: 2012-11-20